Celest Mech Dyn Astr (2008) 102:255–272
DOI 10.1007/s10569-008-9130-0

ORIGINAL ARTICLE

Observation of Hamiltonian chaos in wave–particle interaction

Fabrice Doveil · Alessandro Macor · Anass Aïssi

Received: 16 November 2007 / Revised: 19 February 2008 / Accepted: 3 March 2008 /
Published online: 26 March 2008

Abstract The motion of charged particle in longitudinal waves is a paradigm for the transition to large scale chaos in Hamiltonian systems. Recently a test cold electron beam has been used to observe its non-self-consistent interaction with externally excited wave(s) in a specially designed Traveling Wave Tube (TWT). The velocity distribution function of the electron beam is recorded with a trochoidal energy analyzer at the output of the TWT. An arbitrary waveform generator is used to launch a prescribed spectrum of waves along the slow wave structure (a 4 m long helix) of the TWT. The resonant velocity domain associated to a single wave is observed, as well as the transition to large scale chaos when the resonant domains of two waves and their secondary resonances overlap. This transition exhibits a "devil's staircase" behavior when increasing the excitation amplitude in agreement with numerical simulation. A new strategy for control of chaos by building barriers of transport which prevent electrons to escape from a given velocity region as well as its robustness are also successfully tested. Thus generic features of Hamiltonian chaos have been experimentally observed.

Keywords Hamiltonian chaos · KAM tori · Resonance overlap · Devil's staircase · Traveling wave tube · Large scale chaos (LSC) · Control of chaos

PACS 52.35.Fp · 05.45.−a · 05.60.−k

F. Doveil (✉) · A. Aïssi
Équipe Turbulence Plasma, Physique des Interactions Ioniques et Moléculaires,
UMR 6633 CNRS–Université de Provence, case 321, Centre de Saint-Jérôme,
13397 Marseille cedex 20, France
e-mail: doveil@up.univ-mrs.fr

A. Aïssi
e-mail: aaissi@up.univ-mrs.fr

A. Macor
Association Euratom-CEA, CEA/DSM/IRFM, CEA/Cadarache,
13108 Saint Paul-lez-Durance cedex, France
e-mail: alessandro.macor@cea.fr

1 Introduction

The destruction of KAM tori is at the root of the transition to chaos in non integrable Hamiltonian systems (Arnold 1974). Beside Celestial Mechanics this transition governs the understanding of many physical systems and examples of applications can be found in many branches of physics: beam collimation in particle physics, chaotic mixing in hydrodynamics, plasma confinement in magnetic fusion devices. Another example is the motion of a charged particle in the field of longitudinal waves. This latter case can even be considered as a paradigm for the transition to large scale chaos.

Wave particle interaction is central in the operation of a Traveling Wave Tube (TWT). In such a device a cold electron beam is used to transfer its energy to a wave through self-consistent effects where the wave acts on the beam electrons by electrostatic forces but the modulated beam charge also reacts on the wave propagation and may produce exponential growth of the wave amplitude. Actively developed just after second world war as radar amplifiers, TWTs are still commonly used owing to their great robustness and wide band capability. We present recent experiments in a specially designed TWT where a very low intensity electron beam is used. The beam is unable to self-consistently induce any appreciable wave growth along the length of the device. The beam particles merely behave as test electric charges and we are thus in a good position to observe the motion of charged particles in externally launched waves.

The paper is organized as follows. In Sect. 2, we recall how the 1,5 degree of freedom Hamiltonian system describing the motion of a charged particle in longitudinal waves can be considered as a paradigm for Hamiltonian systems. In Sect. 3, we present the TWT. Section 4 deals with the case where a single wave is launched and the resonant domain associated to the wave in phase space is experimentally measured. Section 5 considers the case of two launched waves: resonance overlap is observed as well as the transition to large scale chaos with the underlying devil's staircase. Section 6 reports how a new strategy of control of chaos has been successfully tested: it consists in adding a small apt perturbation in the form of a third wave to locally restore a KAM barrier in phase space. Section 7 gives our conclusion and states the perspectives opened by this work.

2 A paradigm Hamiltonian

We will restrict to two degrees of freedom Hamiltonian systems. If we consider an integrable Hamiltonian described by $H_0(\mathbf{A})$, where $\mathbf{A} = (A_1, A_2)$ are action variables canonically conjugated to angle variables $\theta = (\theta_1, \theta_2)$, we know that the dynamics evolves periodically or quasi-periodically on invariant tori in phase space. The question that naturally arises is the persistence of these regular structures when the system is perturbed and we consider $H = H_0(\mathbf{A}) + V(\mathbf{A}, \theta)$. KAM (Kolmogorov, Arnold, Moser) theorem gives the right answer (Arnold 1974). Under prescribed hypothesis for the perturbation, and if the perturbation is sufficiently weak, some invariant tori are preserved. When the amplitude of the perturbation increases, more and more tori are destroyed, giving birth to trajectories which are no more confined on tori and may wander chaotically in phase space (Laskar et al. 1992).

We define $\omega(\mathbf{A}) = dH_0/d\mathbf{A}$. We intend to study the motion in the vicinity of a torus characterized by a frequency $\omega(\mathbf{A_r}) = \omega_r$ and related to a value of the action $\mathbf{A}_r$ in the absence of the perturbation. By definition ω_r is normal to the energy curve $H_0(\mathbf{A}) = E$. Let $\mathbf{r}$ be a vector normal to ω_r at $\mathbf{A}_r$, and therefore tangent to the energy curve at this point. Fourier expanding the perturbation, we get

$$V(\mathbf{A},\theta)=\sum_{\mathbf{q}} V_{\mathbf{q}}(\mathbf{A})\times\cos[\mathbf{q}\cdot\theta]. \tag{1}$$

The first approximation consists in replacing $V_{\mathbf{q}}(\mathbf{A})$ by its constant value at $\mathbf{A}_r$ in this expansion. The canonical transformation generated by

$$F(\mathbf{I},\theta)=(\mathbf{A}_{\mathbf{r}}+I_1\mathbf{r}+I_2\omega_{\mathbf{r}})\cdot\theta. \tag{2}$$

defines new variables $\mathbf{I}$ and ϕ and allows to decompose the motion in the frame $(\mathbf{r},\omega_r)$ in the vicinity of $\mathbf{A}_r$. In these new variables the Hamiltonian writes

$$H_r(\mathbf{I},\phi)={\omega_r}^2 I_2+\frac{1}{2}a{I_1}^2+\sum_{\mathbf{q}} V_{\mathbf{q}}(\mathbf{A}_{\mathbf{r}})\times\cos[\alpha_q\phi_1+\beta_q\phi_2], \tag{3}$$

where we dropped the constant term, $a=\mathbf{r}\cdot\overline{\overline{\sigma}}\,\mathbf{r}$ with $\overline{\overline{\sigma}}=d\omega/d\mathbf{A}_{\mathbf{r}}$ and α_q and β_q are the projections of $\mathbf{q}$ on $\mathbf{r}$ and $\omega_{\mathbf{r}}$. With a judicious choice of time origin, the dynamics of variables I_1 and ϕ_1 is described by the time dependent one degree of freedom Hamiltonian system

$$h_r(I_1,\phi_1,t)=\frac{1}{2}a{I_1}^2+\sum_{\mathbf{q}} V_{\mathbf{q}}(\mathbf{A}_{\mathbf{r}})\times\cos[\alpha_q\phi_1-\gamma_q t], \tag{4}$$

where $\gamma_q=-\beta_q{\omega_r}^2$. The first term in this equation can be considered as the kinetic energy of a particle with mass $1/a$ and charge e moving in the potential of electrostatic waves with wavenumber α_q, pulsation γ_q and amplitude $V_{\mathbf{q}}(\mathbf{A}_{\mathbf{r}})/e$.

If, in the previous expansion, we only retain the two terms for which the phase variation is the slowest in the vicinity of $\mathbf{A}_{\mathbf{r}}$, we end up with considering the motion of a charged particle in two waves which therefore appears as a paradigm for the dynamics of two degrees of freedom Hamiltonian systems. With proper normalization of time and space, this Hamiltonian writes

$$h(v,x,t)=\frac{1}{2}v^2-M\times\cos x-P\times\cos\left[k\,(x-t)\right], \tag{5}$$

where v and x are canonically conjugated variables and M, P, and k are constant parameters. It can also describe the motion of a non linear pendulum with periodic forcing. The libration of the pendulum around its stable equilibrium point corresponds to the trapping of the charged particle in the potential well of a single wave with a finite exploration in position; the particle velocity exploration is then limited to the so-called resonant domain centered on the wave phase velocity and with amplitude equal to twice the square root of the wave amplitude with our normalization. The rotation of the pendulum corresponds to the circulation of the charged particle above the potential hills of the wave; this occurs when the particle energy is larger than the amplitude of the wave with our normalization. In the presence of two waves, it is usual to define the overlap parameter

$$s=2\left(\sqrt{M}+\sqrt{P}\right), \tag{6}$$

where $s=1$ corresponds to the overlap of the resonant domains. Numerical calculations of orbits are displayed in Fig. 1 for two different values of s.

For intermediate values of s, islets of stability with regular orbits persist in between the two main resonances associated to the two waves. These secondary resonances can be easily recovered analytically. Let us define by $h_0(J)$ the integrable Hamiltonian that describes, in action-angle variables (J,ψ), the motion of the non linear pendulum associated to a single

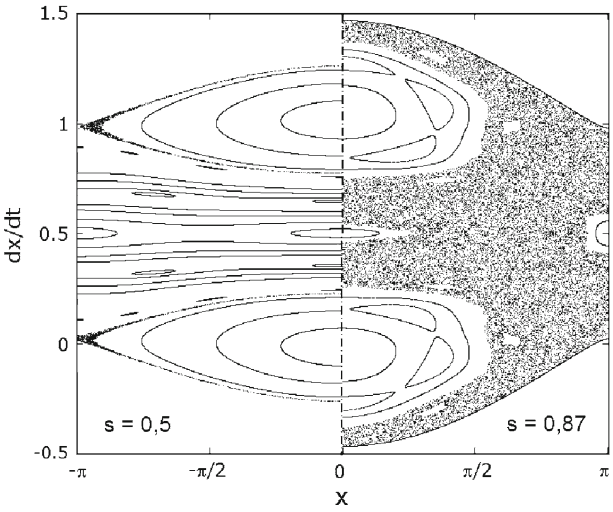

Fig. 1 Poincaré surface of section for the dynamics given by $\ddot{x} = -\varepsilon(\sin(x) + \sin(x - t))$. Left half for $\varepsilon = 1/64$ ($s = .5$) exhibits island chains of secondary resonances at rational velocities $m/(n + m)$; right half for $\varepsilon = 3/64$ ($s = .87$) exhibits large scale chaos. Same 26 initial conditions for both halves

wave ($P = 0$). A Fourier analysis of Eq. 5 allows to describe the motion of a particle in two waves by Hamiltonian

$$h'(J, \psi, t) = h_0(J) - P \sum_n V_n(J) \times \cos\left[(k + n)\,\psi - kt\right], \tag{7}$$

where the coefficients $V_n(J)$ can be determined analytically (Escande and Doveil 1981). We thus exhibit a first set of secondary resonances around velocities $v_n = k/(k + n)$ which appear clearly on the left side of Fig. 1. This is the first step of an iterative process. Letting the secondary resonances play the same role as the two first primary resonances allows to describe the fractal structure of phase space, with the well-known devil's staircase whose steps are limited by persisting Kolmogorov-Arnold-Moser (KAM) tori (Doveil and Escande 1982).

As shown in the right part of Fig. 1 for a larger value of s merging of chaotic regions can lead to the appearance of Large Scale Chaos (LSC) associated to resonance overlap or more precisely to the destruction of the last KAM torus. The resonance overlap criterion $s = 1$ is still commonly used to get an estimate of the threshold for the transition to LSC (Chirikov 1979; Escande 1985). The previous iteration scheme is at the root of an approximate renormalization theory that allows to more precisely address the destruction of KAM tori (Escande and Doveil 1981).

If one considers a beam of initially monokinetic particles having a velocity equal to the phase velocity of one of the waves, this chaotic zone is associated with a large spread of the velocities after some time since the particles are moving in the chaotic sea created by the overlap of the two resonances (Chirikov 1979; Escande 1985). As shown in Fig. 2, the transition to large scale chaos occurs by vertical steps, related to the presence of the nested secondary resonances. Therefore the border of the velocity domain over which the beam is spread exhibits a devil's staircase-like behavior (Macor et al. 2005).

Experimentally, resonance overlap was only observed so far through indirect effects, such as particle heating in plasma physics (Doveil 1981; Skiff et al. 1987). In this paper, we report

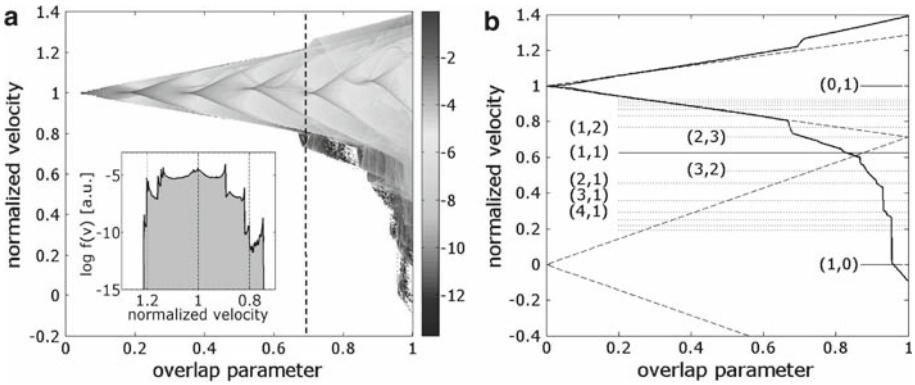

Fig. 2 Numerical devil's staircase. **(a)** Probability distribution function $f(v)$ (with logarithmically scaled color coding) of the velocity for the dynamics given by $\ddot{x} = -\varepsilon(\sin(x) + 0.16\sin\kappa(x-t))$, with $\kappa = 5/3$, as a function of overlap parameter $s = 2.8\sqrt{\varepsilon}$ after a time $t = 24\pi$, i.e. 20 Poincaré stroboscopic periods (inset, $f(v)$ for the value of s indicated by the vertical dashed line). **(b)** Velocity frontiers of $f(v)$ versus s for $t = 24\pi$; dashed oblique lines starting from $v = 0$ and $v = 1$ indicate the primary resonances trapping domains; secondary resonances (n, m) are indicated at rational velocities $m\kappa/(n + m\kappa)$

the direct experimental evidence of the occurrence of this fundamental phenomenon obtained by using a test electron beam in a TWT (Doveil et al. 2005a). This experiment also allowed to observe the above-mentioned fractal structure of Hamiltonian phase space (Macor et al. 2005; Doveil et al. 2006). We will also show how by acting on secondary resonances we can experimentally control chaos (Chandre et al. 2005).

3 Experimental set-up

The experiment is performed in a long Traveling Wave Tube (TWT). TWTs were developed shortly after second world war as radar amplifiers (Pierce 1950; Gilmour 1994). Due to their wide band capability and their robustness, they still play an important role in present days and a standard telecommunication satellite will commonly embark about fifty such devices. Our experimental set-up was inspired by a somewhat unconventional TWT built in San Diego in 1976 to investigate the nonlinear behavior of the small-cold-beam-plasma instability (Dimonte and Malmberg 1978). It consists of three main elements: an electron gun, a slow wave structure (SWS) formed by a helix with axially movable antennas, and an electron velocity analyzer. Figure 3 shows a sketch and a picture of the device.

The electron gun creates a beam, with radius equal to 3 mm, which propagates along the axis of the SWS and is confined by a strong axial magnetic field with a typical amplitude of 0.05 T. Beam currents, $I_b < 1$ mA, and maximal cathode voltages, $|V_c| < 200$ V, can be set independently. Two correction coils provide perpendicular magnetic fields to control the tilt of the electron beam with respect to the axis of the helix.

Waves are launched with an antenna at the gun end of the SWS. With the above parameters, the SWS is long enough to allow nonlinear processes to develop. As sketched in Fig. 4, it consists of a wire helix that is rigidly held together by three threaded alumina rods and is enclosed by a glass vacuum tube. The pump pressure at the ion pumps on both ends of the device is 2×10^{-9} Torr. The 4 m long helix is made of a 0.3 mm diameter Be-Cu wire; its radius is equal to 11.3 mm and its pitch to 0.8 mm. A resistive rf termination at each end of the

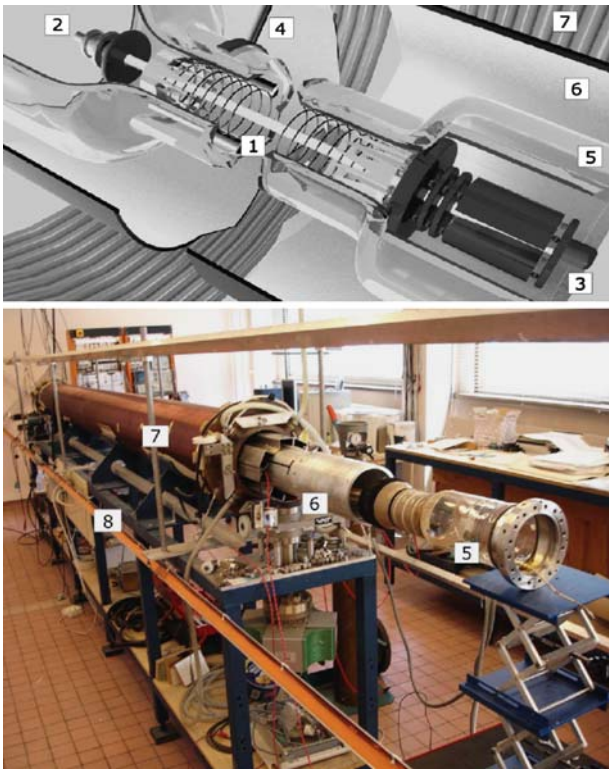

Fig. 3 Sketch of the TWT and picture of the disassembled device: (1) helix, (2) electron gun, (3) trochoidal analyzer, (4) one of four axially movable probes, (5) glass vacuum tube, (6) slotted rf ground cylinder, (7) magnetic coil, (8) square magnetic coils for beam tilt correction

helix reduces reflections. The maximal voltage standing wave ratio is 1.2 due to residual end reflections and irregularities of the helix. The glass vacuum jacket is enclosed by an axially slotted 57.5 mm radius cylinder that defines the rf ground. Inside this cylinder but outside the vacuum jacket are four axially movable antennas which are capacitively coupled to the helix and can excite or detect helix modes in the frequency range from 5 to 95 MHz. Only the helix modes are launched, since empty waveguide modes can only propagate above 2 GHz. These modes have electric field components along the helix axis (Dimonte and Malmberg 1978). Launched electromagnetic waves travel along the helix at the speed of light; their phase velocities, $v_{\phi j}$, along the axis of the helix are smaller by approximately the tangent of the pitch angle, giving 2.8×10^6 m/s $< v_{\phi j} < 5.3 \times 10^6$ m/s. Since the pitch of the helix is much smaller than its radius, the wave propagates along the axis of the helix with a phase velocity which is much smaller than the velocity of light and can be resonant with the electron beam.

The dispersion relation is shown in Fig. 11. Waves on the beamless helix are slightly damped, with $|k_j^{0i}|/|k_j^{0r}| \approx 0.005$ where $k^0 = k^{0r} + \mathrm{i}\, k^{0i}$ is the beamless complex wave number. Further, on the beamless helix, both wave number and damping rate are somewhat position dependent ($|k^{0r}|$ varies by 0.5% and $|k^{0i}|$ varies by 30% over the length of the helix). The TWT has the advantage that the slow wave structure remains linear for the wave amplitudes reached in the experiments; furthermore, it does not introduce noise.

Fig. 4 Sketch of the wave guide and SWS: (A) Beryllium-Copper helix, (B) glass vacuum jacket, (C) threaded alumina rods, (D) slotted RF ground cylinder, (E) antenna/probe

Finally, the cumulative changes of the electron beam distribution are measured with the velocity analyzer, located at the end of the interaction region. This trochoidal analyzer (Guyomarc'h and Doveil 2000) works on the principle that electrons undergo an E × B drift when passing through a region in which an electric field E is perpendicular to a magnetic field B.

Figure 5 shows a typical beam radial profile as measured by scanning the magnetic field of the two perpendicular correction coils used to control the tilt of the electron beam. It shows that the beam propagates along the 4 m long helix preserving its initial homogeneity across the grounded anode hole. The superimposed circle sketches the entrance electrode hole of the trochoidal analyzer. The surrounding halo is the result of selection of the gyrating electrons passing through the electrodes holes and its width gives a measurement of twice the electron Larmor radius (Macor 2007).

In this paper, we consider a very weak cold beam. The beam intensity is sufficiently weak that the unstable waves exhibit a negligible growth upon the length of the experiment. The beam electrons can thus be considered as test particles submitted to externally excited waves with almost constant amplitude and the Hamiltonian dynamics of a charged test particle can be experimentally explored.

4 Single wave

For a single wave, characterized by its amplitude ϕ and frequency f launched by a fixed antenna at a given distance from the output of the device, the time-averaged velocity distribution function (*vdf*) of the test electron beam is measured at the device output. The plots of the subsequent figures are the result of superposing measurements obtained by varying one of the controlling parameter keeping all the others constant. For each value of the varying control parameter (*vcp*), the output beam *vdf* is recorded after interaction of the test beam with the

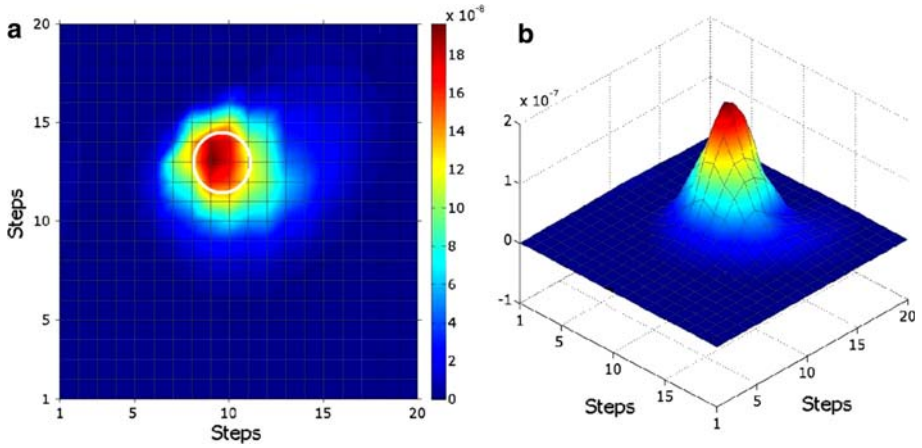

Fig. 5 Radial profile of a test cold beam at the output of the TWT

wave propagating along the helix: the *vdf* is obtained by scanning the retarding voltage with a step of 61 mV. The zero level of each *vdf* is defined as the mean trochoidal collector current averaged over 50 velocities in the tail of the *vdf*. Each beam *vdf* is then normalized to keep the beam current constant. The final plot is obtained after an appropriate Matlab treatment of the recorded output *vdfs*, giving a 3D plot of the *vdf* in (vcp, v) plane, or a 2D contour plot of the amplitude of the distribution function in (vcp, v) plane.

4.1 Beam trapping

As explained before, Fig. 6 gives a 2D plot of the *vdf* detected by the trochoidal analyzer when the varying control parameter is the wave amplitude for the case when the beam is trapped inside the potential trough of the wave (libration of the classical non-linear pendulum). Indeed the test beam with intensity $I_b = 120$ nA has an entrance velocity equal to the phase velocity of the wave at 40 MHz launched by a fixed antenna at $L = 230$ cm from the device output. In Fig. 6 the 2D plot of the amplitude of the *vdf* detected by the trochoidal analyzer is the result of superposing measurements obtained for different wave amplitudes of the single wave varying from 0 to 45 mV by steps of 3 mV.

We first notice that the shape of the velocity domain in which the test beam electrons are spread increases like the square root of ϕ. This is explained by the fact that the beam is trapped in the potential troughs of the wave. From the measured antenna coupling coefficients (Malmberg et al. 1966), the helix wave amplitude ϕ can be estimated. The resonant or trapping domain in velocity can thus be deduced and is indicated by the continous lines in Fig. 6 which correspond to $v_\phi \pm 2\sqrt{\eta\phi}$ where η is the electron charge to mass ratio. We observe a very good agreement with measurement.

Another feature appearing in Fig. 6 is a further velocity bunching of the electrons around their initial velocity for an applied amplitude equal to 850 mV. This phenomenon is also related to the trapping of the electrons in the wave. If we refer to the rotating bar model (Mynick and Kaufman 1978) to describe the trapped electrons motion, we expect oscillations between small spread in velocity and large spread in position (corresponding to initial conditions for a cold test beam) to large spread in velocity and small spread in position after half a bounce or trapping period equal to $T_b/2 = v_\phi/2(f\sqrt{\eta\phi})$. To the bounce period, we can

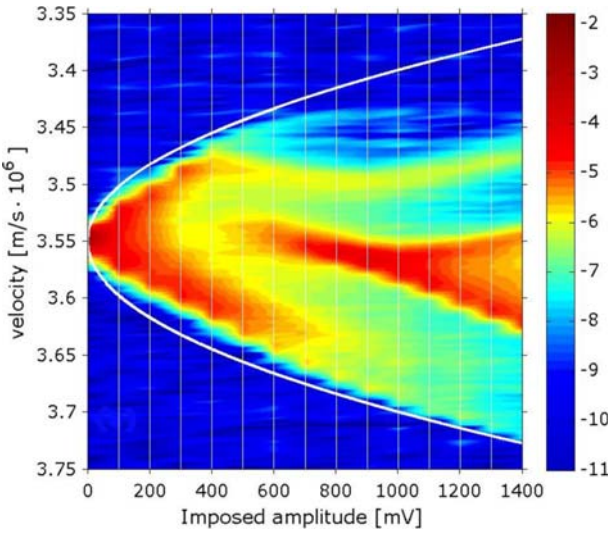

Fig. 6 Measured velocity domain for a test beam ($I_b = 120$ nA, $v_b = 3.55 \times 10^6$ m/s) trapped in a single wave at 40 MHz with trapping domain (continuous curve) for increasing amplitude

associate a bounce length $L_b = v_\phi T_b$. An estimate of the wave amplitude ϕ can be obtained by determining the emitting probe coupling coefficient C using 3 probes measurements (Malmberg et al. 1966). We found $C = 0.032$ for a wave at 40 MHz, and for an amplitude of the signal on the emitting probe equal to 850 V, we obtain $\phi = 27$ mV. For this value, we get $L_b/2 = 230$ cm which is precisely the interaction length L of Fig. 6. We thus confirm that Fig. 6 is displaying the trapping of the test beam in the single wave.

4.2 Resonant domain

The 2D amplitude plot of Fig. 7 is obtained by using the entrance test cold beam velocity as the *vcp* and keeping the wave amplitude constant $\phi = 150$ mV for a fixed interaction length $L = 370$ cm. To be more accurate, Fig. 7 is obtained by scanning the entrance energy of the test beam from 32 to 65 eV by step of 0.5 eV. Two different regions are clearly apparent in Fig. 7. For small or large values of v_b, the distribution remains centered around its initial velocity along the bisectrix of Fig. 7 with a small spread due to the electrons sloshing around v_b. For intermediate values of v_b, the *vdf* is observed to spread over a wide domain. This is explained by the fact that in the velocity domain explored by Fig. 7, the beam can be trapped in the potential troughs of the wave. The central velocity of the domain where the distribution is significantly spread is indeed $v_0 = 4.06 \times 10^6$ m/s which is the phase velocity of the 30 MHz wave given by the dispersion relation of the helix and is indicated by a star in Fig. 7. An estimate of the wave amplitude ϕ can be obtained by determining the emitting probe coupling coefficient C using 3 probes measurements (Malmberg et al. 1966). We found $C = 0.065$ for a wave at 30 MHz, and since the amplitude of the signal on the emitting probe is $A = 2.3$ V, we obtain $\phi = 150$ mV. The broken lines in Fig. 7 correspond to $v_0 \pm 2\sqrt{\eta\phi}$ and define the upper and lower velocity limits of the resonant region assuming a traveling wave with constant amplitude ϕ. We observe that these broken lines correctly limit the domain where *vdf* is no longer symmetrical around v_b and this domain can therefore be seen as the measured resonant zone.

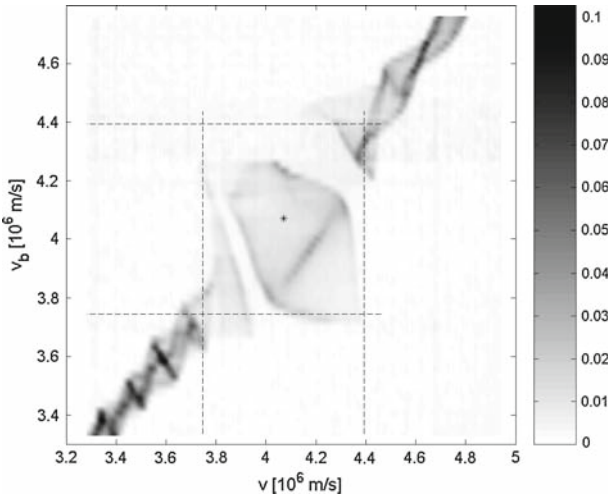

Fig. 7 Measured resonant velocity domain for a single wave at 30 MHz

From the wave amplitude, we can compute the trapping or bounce frequency of the electrons in the bottom of the wave equal to $\omega_b = k\sqrt{\eta\phi}$ from which a bounce length $L_p = 2\pi v_b/\omega_b$ is estimated. From the above value for ϕ we get $L_p = 3.2$ m. This shows that the TWT is sufficiently long to observe one complete trapping oscillation of the test beam in the wave. This also explains why there are intricate structures inside the trapping region of Fig. 7: a little more than one trapping oscillation can be observed in the device for this frequency and the mixing due to anharmonicity of trapping oscillations is not complete. In conclusion Fig. 7 gives a nice direct experimental evidence of the velocity resonant domain for wave–particle interaction. By varying the amplitude of the launched wave, we also checked that the width of the resonant domain scales as predicted by wave trapping theory.

5 Two waves

We now consider the case where two waves at different frequencies are launched by the same fixed antenna.

5.1 Resonance overlap

Two waves at frequencies $f_1 = 30$ MHz and $f_2 = 40$ MHz are launched with amplitudes $A_1 = 0.7$ V and $A_2 = 0.8$ V respectively. The measured dispersion relation gives $v_{\phi 1} = 4.06 \times 10^6$ m/s (resp. $v_{\phi 2} = 3.55 \times 10^6$ m/s) for the phase velocity of the wave at frequency f_1 (resp. f_2). Figure 8a is obtained in the same way as Fig. 7. We observe well separated resonant velocity domains centered around $v_{\phi 1}$ and $v_{\phi 2}$ (shown as stars in Fig. 8a) since, for initial velocities of the test beam in between the two resonant domains, the velocity distribution does not spread very much around its initial velocity. As above, from the measured probe coupling coefficients equal to 0.065 (resp. 0.04) at 30 MHz (resp. 40 MHz), the two resonant or trapping domains in velocity can be estimated and are indicated by the broken lines in Fig. 8a. We again observe that the regions where the perturbed distribution functions get broader correspond to these domains. According to Eq. 6, this case corresponds to an overlap

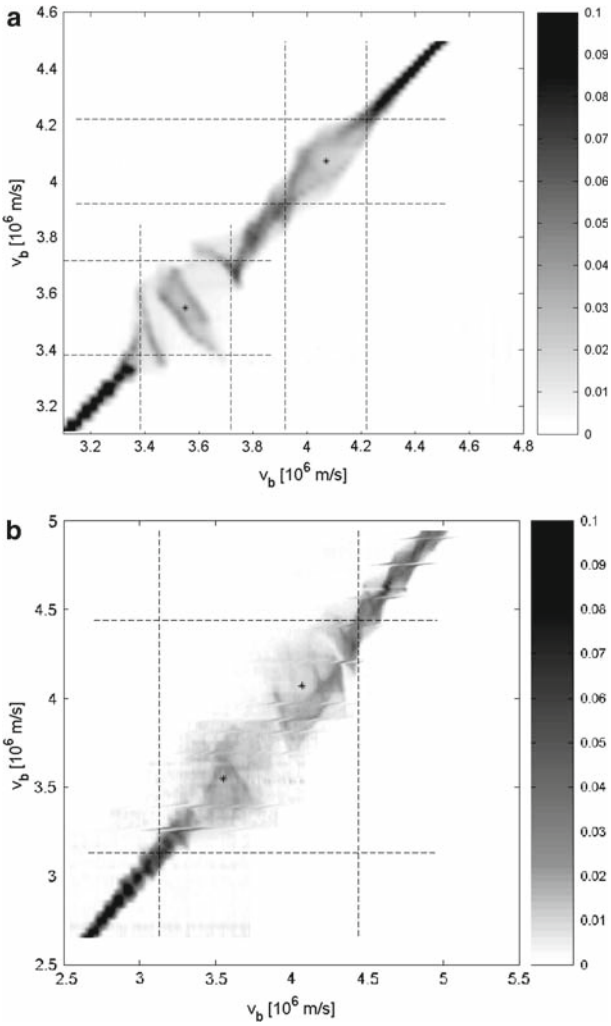

Fig. 8 Measured resonant velocity domain for two waves at 30 and 40 MHz: **(a)** $s = 0.63$, **(b)** $s = 1.5$

parameter $s = 0.63$ below the theoretical threshold for LSC (Escande and Doveil 1981). We therefore cannot expect LSC, in agreement with what is observed on Fig. 8a.

On the contrary, Fig. 8b corresponds to larger amplitudes of the two launched waves respectively equal to $A_1 = 3.0\,\mathrm{V}$ and $A_2 = 6.25\,\mathrm{V}$. As expected, we observe an increase of the velocity zone in which the normalized distribution function is considerably spread. Furthermore we no longer observe, as we do in Fig. 8a, a peaking of the distribution function for a velocity equal to $(v_{\phi 1} + v_{\phi 2})/2 = 3.80 \times 10^6$ m/s and the two resonant domains are merging in a single one. The upper (resp. lower) limit of the large resonant domain agrees well with the velocity indicated by broken lines in Fig. 8b and defined as $v_{\phi 1} + 2\sqrt{\eta \phi_1}$ (resp. $v_{\phi 2} - 2\sqrt{\eta \phi_2}$) obtained by using the emitting probe coupling coefficients as above. This case corresponds to an overlap parameter $s = 1.5$, well above the theoretical threshold for LSC. We thus have on Fig. 8b a direct experimental indication of resonance overlap.

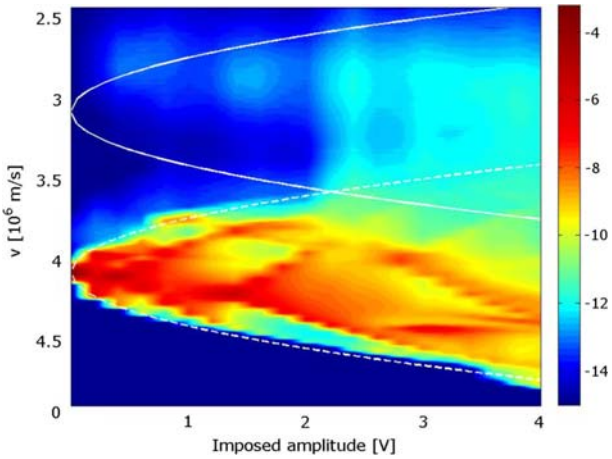

Fig. 9 2D contour plot of the measured *vdf* (with logarithmically scaled color coding) of a test beam ($I_b = 10\,\text{nA}$) interacting with two waves at 30 MHz and 60 MHz with trapping domains (continuous and dashed curves) for increasing amplitude and fixed interaction length $L = 3.6\,\text{m}$, $v_b = 4.06 \times 10^6\,\text{m/s}$

5.2 Transition to large scale chaos (LSC)

In the next experiment, we apply, on an antenna chosen for its strongest coupling with the helix and located at $L = 3.5\,\text{m}$ from the device output, a signal made of two components: one at 30 MHz, and one at 60 MHz. According to the helix dispersion relation, two travelling waves propagate along the helix, the former with a phase velocity $v_{\varphi 1} = 4.06 \times 10^6\,\text{m/s}$ as before, the latter with a different phase velocity $v_{\varphi 2} = 3.08 \times 10^6\,\text{m/s}$ (the fact that the second wave is a harmonic of the first one in the laboratory frame is irrelevant in the beam frame).

Figure 9 is obtained in the same way as Fig. 6 for a test beam, with intensity $I_b = 10\,\text{nA}$ and initial velocity $v_b = v_{\varphi 1}$, whose *vdf* is measured at the outlet of the tube after its interaction with the two propagating helix modes. As in Fig. 6 the continuous (resp. dashed) parabola shows the trapping velocity domain associated to the helix mode at 60 MHz (resp. 30 MHz). As it appears clearly, the amplitudes of the two modes have been appropriately chosen such that these trapping domains approximately have the same velocity extension when taking into account the coupling coefficient of the antenna at the two working frequencies. We observe that, for a threshold amplitude exceeding the amplitude corresponding to overlap of the trapping domains, the *vdf* exhibits a strong velocity spread. Electrons initially trapped inside the potential well of one of the helix modes can escape the trapping domain and explore a much wider velocity region in phase space. According to their initial velocity, electrons can be strongly decelerated. We can therefore relate this behavior to the transition to large scale chaos for the motion of a charged particle in two electrostatic waves.

5.3 Devil's staircase

We again apply an oscillating signal at a single frequency of 30 MHz for an interaction length $L = 3.5\,\text{m}$. But we now consider a test beam, with intensity $I_b = 10\,\text{nA}$ and initial velocity $v_b = 2.7 \times 10^6\,\text{m/s}$ much lower than v_φ, the phase velocity of the helix mode at 30 MHz. Figure 10a is obtained in the same way as Fig. 9. The continuous parabola indicates the velocity domain associated to particle trapping in the potential troughs of the helix mode

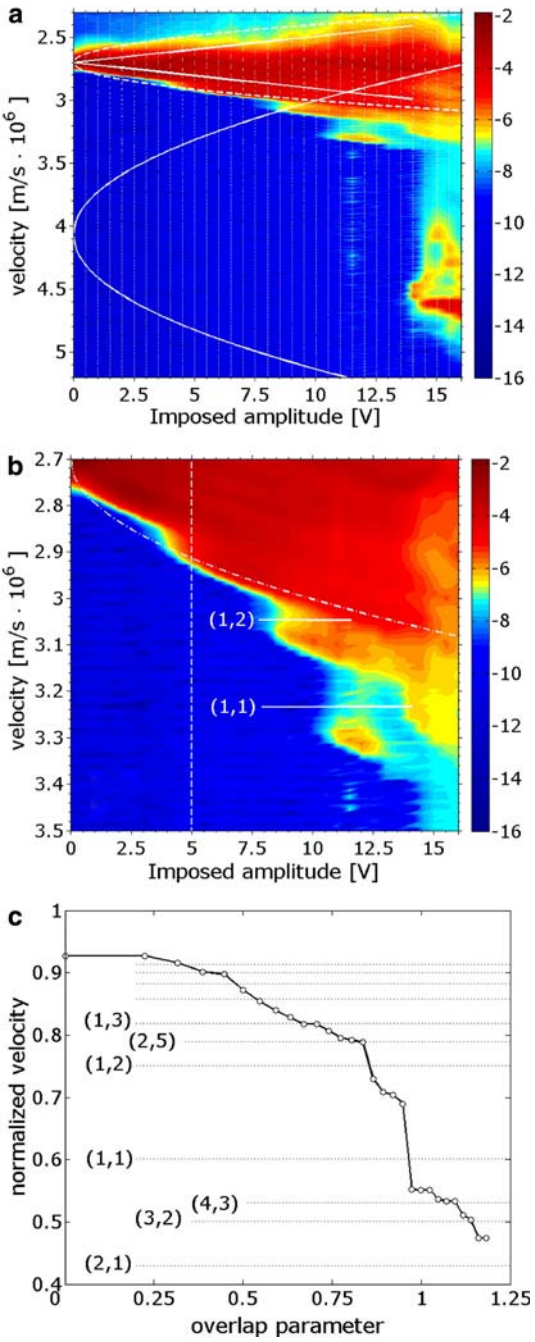

Fig. 10 **(a)** 2D contour plot of the measured *vdf* (with logarithmically scaled color coding) of a test beam ($I_b = 10\,\text{nA}$, $v_b = 2.7 \times 10^6\,\text{m/s}$) with applied signal at 30 MHz for increasing amplitude and fixed interaction length $L = 3.6\,\text{m}$ (trapping domains of helix and beam modes are indicated by continuous and dashed parabolas); **(b)** Zoom of **(a)**; **(c)** Normalized upper velocity frontier of $f(v)$ versus overlap parameter s; velocity normalization is such that $v = 0$ (resp. 1) stands for the helix (resp. beam) mode phase velocity; secondary resonances (n, m) are indicated at velocities $m\kappa/(n + m\kappa)$ with $\kappa = v_\varphi / v_b$

at 30 MHz. Since the initial beam velocity lies far out of this domain we expect that, for moderate wave amplitude, the beam electrons will experience a mere velocity modulation around their initial velocity, with a modulation amplitude increasing linearly with the applied signal amplitude. This behavior has been studied in Doveil et al. (2005b) and would generate two main peaks around the (oblique straight) continuous lines originating in v_b.

In fact we observe that the electrons spread over a velocity domain with typical width increasing as the square root of the applied signal amplitude as shown by the dashed parabola. This strongly recalls the results of Fig. 6. Indeed the applied signal generates two waves: a helix mode with a phase velocity v_φ, and a beam mode with a phase velocity equal to the beam velocity v_b. The beam mode with phase velocity v_b is actually the superposition of two indistinguishable modes with pulsation $\omega = kv_b \pm \omega_b$ corresponding to the beam plasma mode with pulsation $\omega_b = [n_b e^2/(m\epsilon_0)]^{1/2}$ for a beam with density n_b, Doppler-shifted by the beam velocity v_b, merging in a single mode since $\omega_b \ll \omega$ in our conditions (Pierce 1950; Gilmour 1994). Thus Fig. 10a shows the test electrons trapping into the beam mode. This is confirmed by a careful analysis of Fig. 10a which exhibits the same velocity bunching of the electrons around their initial velocity as in Fig. 6, for amplitudes obtained by equating the interaction length to a multiple of half the trapping length. One also notices that the amplitude of the beam mode is lower than the amplitude of the launched helix mode; this explains why its influence has been neglected in the previous analysis of Fig. 9 where two helix modes are externally excited. Since, when we increase the applied signal amplitude in Fig. 10a, the two trapping domains of the helix and the beam mode overlap, we observe the same behavior as in Fig. 9. Above a certain applied signal amplitude threshold the distribution function spreads over a much wider velocity domain, and electrons can be strongly accelerated.

Another striking feature appears in Fig. 10a, which is best emphasized in the zoom of Fig. 10b. The transition to large velocity spread does not occur continuously but rather occurs by steps when the applied signal amplitude increases. Plateaus are formed in the measured *vdf* for the maximum interaction length. A closer look at Fig. 9 also reveals the presence of such steps in the zone between the two main resonances in the case of two independently launched waves with equal amplitudes. This generic phenomenon is related to the intrinsic structure of Hamiltonian phase space for non integrable systems briefly recalled in Sect. 2. Figure 10a is the experimental counterpart of Fig. 2a, b. Figure 10c shows the upper border of the measured *vdf* with superimposed the positions of the unperturbed higher order resonances velocities given by $v_{nm} = m\kappa/(n + m\kappa)$ with $\kappa = v_\varphi/v_b$ (Doveil et al. 2006). It exhibits the first steps of the "devil's staircase" in phase space.

6 Control of chaos

We have used the same experimental conditions to test a new method of control of chaos which aims at building barriers in phase space and hence confine all the trajectories rather than following them individually. The reduction of chaotic behaviors is achieved by using a small apt perturbation of the system which keeps its Hamiltonian structure. For the Hamiltonian given by Eq. 5, we use as a control term the opposite of the first term $n = 1$ in the Fourier series of Eq. 7 (Chandre et al. 2005). This control term corresponds to the beating of the two main waves. Physically it consists in destroying the largest secondary island chain $(n = 1, m = 1)$ in between the two main resonances of Fig. 1 which constitutes the largest step of the previously observed staircase. In fact this control term is the most important term of a more precise control theory (Chandre et al. 2006). Using this approximate control term does not guarantee the existence of an invariant torus. However since the difference between

this term and the exact one is small, it is expected that for a Chirikov parameter s not too large, the approximate control term is still effective in reducing chaos.

The challenge is then to be able to launch three different waves with well controlled amplitude, frequency and phases, the third one corresponding to the beating of the first two ones with amplitude prescribed by control theory, pulsation $\omega_1 + \omega_2$, wave numbers $k_1 + k_2$, and phase $\chi_1 + \chi_2$. This can be done using an arbitrary wave form generator. These three waves must correspond to TWT modes. Due to the form of the dispersion relation, working with pure helix modes would prove impossible. Working with the helix mode and the beam mode at the same frequency as explained in the previous section provides an easy way to satisfy the resonance condition. As shown in Fig. 11, the beam velocity (the phase velocity of the beam mode) is then accurately set by the frequency choice.

Figure 12a shows the test beam *vdf* measured at the output of the TWT in the absence of externally excited wave. The beam remains extremely narrow. We then apply an oscillating signal at a frequency of 30 MHz on an antenna at the entrance of the TWT. As explained before, this signal generates two waves: a helix mode with a phase velocity equal to $v_\phi = 4.06 \times 10^6 m/s$; a beam mode with a phase velocity equal to the beam velocity v_b. Figure 12b shows the measured *vdf* of the beam after interacting with these two modes over the length of the TWT. The right (resp. left) band gives the size of the resonant domain determined as the trapping velocity width of the helix (resp. beam) mode $v_\phi \pm 2\sqrt{eV_h/m}$ (resp. $v_b \pm 2\sqrt{eV_b/m}$) where $V_h = 2.33V$ $(resp. V_b = 0.17V)$ is the amplitude of the helix (resp. beam) mode determined both from antennas and beam measurements. These two domains slightly overlap and the breakup of invariant KAM tori results in a large spread of the initially narrow beam of Fig. 12a over the chaotic region (note the change in scale for the vertical axis); only two small bumps remain which correspond to nested regular regions in phase space as shown in Fig. 1. The beam velocity of Fig. 12 has been chosen in such a way that the wave number of the beating mode at 60 MHz properly satisfies the helix dispersion relation as shown by

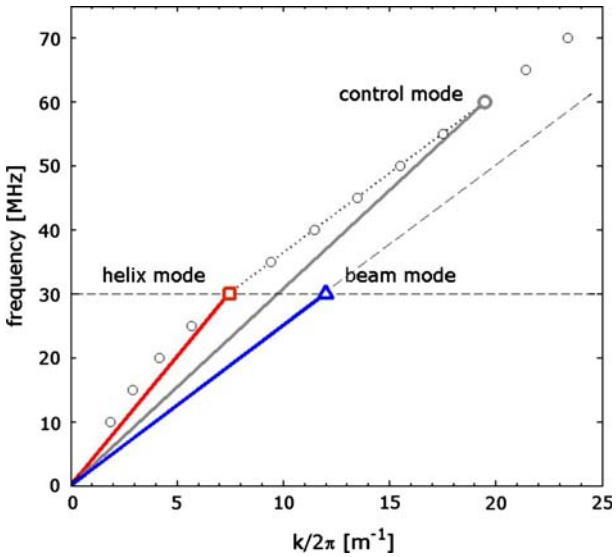

Fig. 11 Resonance condition: TWT dispersion relation (circles) with the helix mode (square) and the beam mode (triangle) at the same frequency. The beating of these two modes is the control mode which must belong to the helix dispersion curve

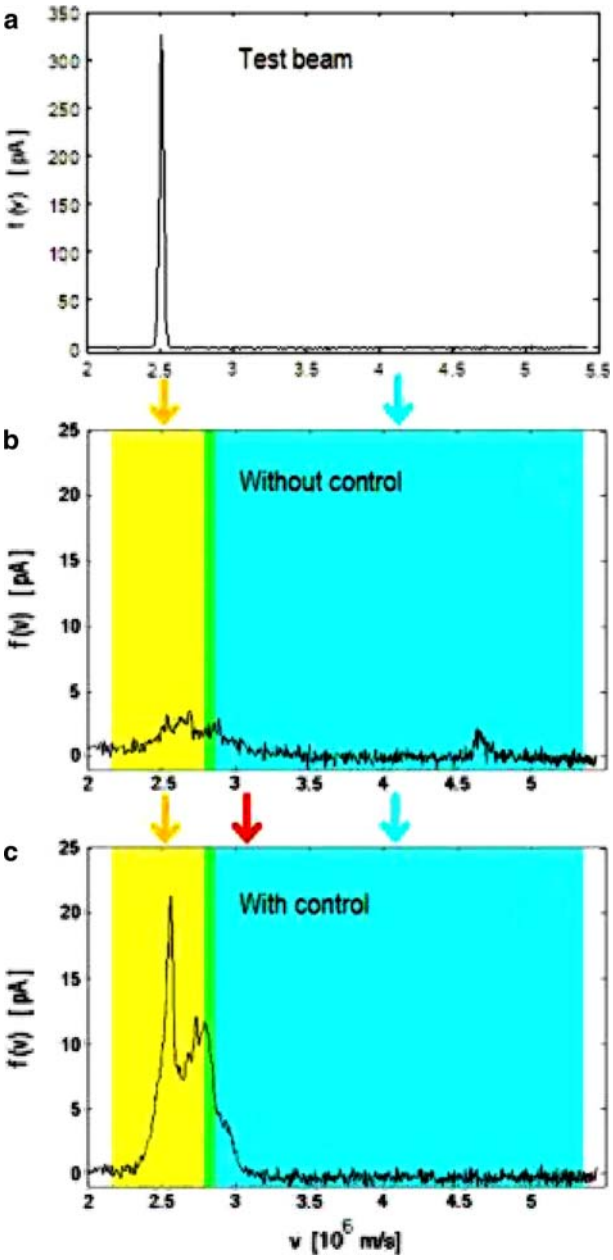

Fig. 12 Beam velocity distribution function at the output of the TWT: **(a)** test beam ($I_b = 50\,\text{nA}$) without electrostatic wave, **(b)** with helix mode [dark gray (blue)] and beam mode [light gray (yellow)] at 30 MHz [phase velocity given by upper arrow and trapping domain of each mode given by shaded (coloured bands)], **(c)** with an additional controlling wave at 60 MHz and phase velocity given by middle (red) upper arrow

Figure 11. We then launch with the arbitrary wave form generator an additional wave at this frequency with the amplitude given by the resonant term $n = 1$ in Eq. 7 and a well-defined phase with respect to the main signal. As observed on Fig. 12c where the middle(red) arrow indicates the phase velocity v_c of the controlling wave, the beam recovers a large part of its initial kinetic coherence and does not spread in velocity beyond v_c. This control of the beam coherence is realized with an additional cost of energy which corresponds to less than 1% of the initial energy of the two-wave system. We stress the importance of a fine tuning of the control term. The robustness of the method has been further tested in a situation of stronger chaos (Macor et al. 2007a).

7 Conclusion and perspectives

The use of a TWT allowed us to explore experimentally the fractal phase space of the paradigm Hamiltonian describing the motion of a charged particle in a spectrum of longitudinal waves. The main features of non integrable systems have thus been recovered. The deep knowledge of the system opened the way to the implementation of a method to channel chaos in phase space by building barriers to chaotic diffusion.

A further development of the experiment would be to use bunches of electrons instead of a continuous beam. By controlling the phase of the electron bunches with respect to the phase of an injected wave, a still better exploration of the dynamics of test electrons could be achieved. This very challenging project is under progress (Macor et al. 2007b).

The results reported in this paper were obtained with a very low intensity test electron beam. By gradually increasing the beam intensity, it is now possible to tackle the fundamental question of the role of chaos when self-consistent effects set in. Beyond the physics of electron devices, it is also a very important question in plasma physics where collective motion of charged particles can induce the growth of unstable waves. An Hamiltonian description is still valid where conjugate variables can be used to describe the coupled evolution of both charged particles and electric fields (Elskens and Escande 2003).

Acknowledgements The authors are grateful to Y. Elskens and D.F. Escande for fruitful discussions and to D. Guyomarc'h and B. Squizzaro for technical assistance. This work is supported by Euratom/CEA. A. Macor benefited from a grant by Ministère de la Recherche and A. Aïssi benefits from CIFRE grant $n^{o}647/2005$ during this work.

References

Arnold, V.I.: Mathematical Methods of Classical Mechanics. Nauka, Moscow (1974)
Chandre, C., Ciraolo, G., Doveil, F., Lima, R., Macor, A., Vittot, M.: Channeling chaos by building barriers. Phys. Rev. Lett. **94**, 074101 (2005)
Chandre, C., Vittot, M., Ciraolo, G., Ghendrih, P., Lima, R.: Control of stochasticity in magnetic field lines. Nuclear Fusion **46**, 33 (2006)
Chirikov, B.V.: A universal instability of many dimensional oscillator systems. Phys. Rep. **52**, 263–379 (1979)
Dimonte, G., Malmberg, J.H.: Destruction of trapping oscillations. Phys. Fluids **21**, 1188–1206 (1978)
Doveil, F.: Stochastic plasma heating by a large-amplitude standing wave. Phys. Rev. Lett. **46**, 532–534 (1981)
Doveil, F., Escande, D.F.: Fractal diagrams for non-integrable Hamiltonians. Phys. Lett. **90A**, 226–230 (1982)
Doveil, F., Auhmani, Kh., Macor, A., Guyomarc'h, D.: Experimental observation of resonance overlap responsible for Hamiltonian chaos. Phys. Plasmas (Lett.) **12**, 010702 (2005a)
Doveil, F., Escande, D.F., Macor, A.: Experimental observation of nonlinear synchronization due to a single wave. Phys. Rev. Lett. **94**, 085003 (2005b)

Doveil, F., Macor, A., Elskens, Y.: Direct observation of a "devil's staircase" in wave–particle interaction. Chaos **16**, 033103 (2006)
Elskens, Y., Escande, D.F.: Microscopic Dynamics of Plasmas and Chaos. IoP Publishing, Bristol (2003)
Escande, D.F.: Stochasticity in classical Hamiltonian systems: universal aspects. Phys. Rep. **121**, 165–261 (1985)
Escande, D.F., Doveil, F.: Renormalization method for computing the threshold of the large-scale stochastic instability in two degrees of freedom Hamiltonian systems. J. Stat. Phys. **26**, 257–284 (1981)
Gilmour, A.S. Jr.: Principles of Travelling Wave Tubes. Artech House, Boston, London (1994)
Guyomarc'h, D., Doveil, F.: A trochoidal analyzer to measure the electron beam energy distribution in a traveling wave tube. Rev. Sci. Instrum. **71**, 4087–4091 (2000)
Laskar, J., Froeschle, C., Celletti, A.: The measure of chaos by the numerical analysis of the fundamental frequencies—application to the standard mapping. Physica D **56**, 253–269 (1992)
Macor, A.: D'un faisceau test à l'auto-cohérence dans l'interaction onde-particule. PhD dissertation, Université de Provence (2007)
Macor, A., Doveil, F., Elskens, Y.: Electron climbing a "devil's staircase" in wave–particle interaction. Phys. Rev. Lett. **95**, 264102 (2005)
Macor, A., Doveil, F., Chandre, C., Ciraolo, G., Lima, R., Vittot, M.: Channeling chaotic transport in a wave–particle experiment. Eur. Phys. J. D **41**, 519–530 (2007a)
Macor, A., Doveil, F., Garabedian, E.: Electron packets to investigate nonlinear phenomena in wave–particle interaction. Nonlinear Phenomena in Complex Systems **10**, 180–183 (2007b)
Malmberg, J.H., Jensen, T.H., O'Neil, T.M.: Plasma Physics and Controlled Nuclear Fusion Research, vol 1. pp. 683 IAEA, Vienna (1966)
Mynick, H.E., Kaufman, A.N.: Soluble theory of nonlinear beam-plasma interaction. Phys. Fluids **21**, 653–663 (1978)
Pierce, J.R.: Travelling Wave Tubes. Van Nostrand, New York (1950)
Skiff, F., Anderegg, F., Tran, M.Q.: Stochastic particle-acceleration in an electrostatic wave. Phys. Rev. Lett. **58**, 1430–1433 (1987)